JOURNAL OF MATERIALS SCIENCE 29 (1994) 4651–4658

The mechanical properties of ternary composites of polypropylene with inorganic fillers and elastomer inclusions

J. JANCAR, A. T. DIBENEDETTO
Institute of Materials Science, University of Connecticut, Storrs, CT 06269, USA

The effect of elastomer volume fraction and phase morphology on the elastic modulus of ternary composites polypropylene (PP)/ethylene–propylene rubber (EPR)/inorganic filler containing 30 vol % of either spherical or lamellar filler has been investigated. Phase morphology was controlled using maleated polypropylene (MPP) and/or maleated ethylene–propylene elastomer (MEPR). As revealed by SEM observations, composites of MPP/EPR/filler exhibit separation of the filler and elastomer and good adhesion between MPP and the filler, whereas composites of PP/MEPR/filler exhibit encapsulation of the filler by MEPR. Composite models were utilized to estimate upper and lower bounds for the elastic modulus of these materials, which is strongly dependent on the morphology of the ternary composite. A model based on the Kerner equation for perfect separation of the soft inclusions and rigid fillers gives a good prediction of the upper limit for relative elastic modulus as a function of filler and elastomer volume fractions. The lower limit, achieved in the case of perfect encapsulation, depends significantly on the particle shape. Good agreement was found between experimental data and lower limits predicted using the Halpin–Tsai equation for lamellar filler and the Kerner–Nielsen equation for spherical filler. In order to calculate reinforcing efficiency of the core–shell inclusions, the finite element method (ANSYS 4.4A, GT STRUDL) has been used.

1. Introduction

With new emerging polymerization processes, polypropylene (PP) becomes an attractive candidate for numerous engineering applications. The mass application of PP in automobiles, mass transportation vehicles, household appliances and the construction industry requires stiffness and fracture toughness similar to those of engineering plastics (ABS, polycarbonate, etc.). In some cases reduced flammability is an additional requirement. Binary PP/filler composites and PP/elastomer blends exhibit either increased stiffness or improved fracture toughness usually at the expense of one or the other.

Ternary composites of PP and modified PP matrices, containing both rigid filler and soft elastomer, provide materials that can be both stiffer and tougher than the neat matrix. The morphology of the ternary blend will depend strongly on mixing conditions, the rheology and surface energies of the constituents and the geometry of the rigid fillers. The limits of ideal behaviour, however, are determined by thermodynamic considerations. For example, when PP and a high surface energy filler are mixed with an elastomer with higher surface energy than that of PP, such as maleated ethylene–propylene rubber (MEPR), the most stable morphology will be that of rigid filler inclusions encapsulated in shells of the elastomer and dispersed in the PP matrix. On the other hand, if a maleated PP (MPP) is used as a matrix with low surface energy ethylene–propylene rubber (EPR), encapsulation of the filler by the elastomer will be supressed, resulting in a morphology of rigid filler embedded in a matrix of MPP in which the elastomer particles are dispersed as a separate phase. Thus, two limiting cases with entirely different mechanical properties can be attained:

(i) perfect separation of the filler and elastomer dispersed in the matrix; and

(ii) perfect encapsulation of the filler by the elastomer and the two-phase particles dispersed in the matrix.

In this paper we report the stiffness and toughness of ternary composites of PP and MPP containing inorganic fillers of calcium carbonate ($CaCO_3$) and magnesium hydroxide ($Mg(OH)_2$) along with elastomeric inclusions of ethylene–propylene copolymer (EPR) and maleated EPR (MEPR). Analytical models will be used to determine the upper and lower bounds of stiffness and experimental data on stiffness and impact strength will be reported to describe the conditions under which an increase in both stiffness and toughness can be achieved.

2. Experimental procedure

Commercial polypropylene Mosten 58.412 (Chemopetrol Litvinov, Czechoslovakia), melt index 4 g/10 min (230 C, 21.6 N), was used as a matrix.

0022–2461 © *1994 Chapman & Hall*

Maleated PP (MPP) (Chemopetrol, Research Institute of Macromolecular Chemistry, Brno, Czechoslovakia) was used to modify the matrix through addition of maleic anhydride (MAH) groups. PP and MPP were mixed in a PLO 651 Brabender Plasticorder to achieve the required concentration of MAH in the matrix. Ethylene–propylene copolymer Dutral CO 054 (Himont, Italy), $T_g = -57\,^{\circ}C$, $M_w = 180\,000\,g\,mol^{-1}$, was used as an elastomer. A maleated version of EPR Dutral CO 054 (MEPR, Chemopetrol, Research Institute of Macromolecular Chemistry, Brno, Czechoslovakia) was mixed with EPR to achieve the required concentration of MAH in the elastomer. Two batches of disc-like (square-platelet) shaped particles of magnesium hydroxide ($Mg(OH)_2$) with an average aspect ratio (length to thickness) of 5 and specific surface areas of 7 and $18\,m^2\,g^{-1}$ (Research Institute of Macromolecular Chemistry, Brno, Czechoslovakia) and particles of calcium carbonate ($CaCO_3$) Durcal 2 (Omya, Switzerland) with average particle diameter of 3.6 μm and specific surface area of $2.5\,m^2\,g^{-1}$ were used as fillers. Untreated fillers were used in order to avoid the effects of commonly utilized low molecular weight surface treatments. Two series of PP/filler/EPR composites were prepared using a PLO 651 Brabender Plasticorder (200 °C, 10 min, 50 r.p.m.). The first series, consisting of 60 vol % PP, 30 vol % $Mg(OH)_2$ and 10 vol % EPR, was prepared with different concentrations of maleic anhydride (MAH) in either the matrix (MPP) or elastomer (MEPR). The second series possessed a constant filler volume fraction of 0.3 while the elastomer volume fraction was varied from 0–0.16. The amount of MAH in materials of the second series was chosen to ensure either maximum separation by maleating the polypropylene to an optimum MAH content or maximum encapsulation by maleating the EPR elastomer to its optimum MAH content. Specimens for mechanical tests were cut from compression-moulded sheets of the compounded materials. Elastic modulus at room temperature was determined using an Instron 4302 Tensile Tester at the strain rate of $1\,min^{-1}$. Reported values were averaged from five specimens with an experimental variation of the order of ± 5%. Fracture surfaces were examined using an AMRAY IV Scanning Electron Microscope (Amray, USA). Dynamic mechanical moduli were measured using an MkII DMTA (Polymer Laboratories, UK) over a temperature range of −100 to 100 °C at 1 Hz.

3. Prediction of elastic moduli for the ternary composites

3.1. Upper bound for elastic modulus: perfect separation

An upper bound for the elastic modulus of a ternary composite of PP filled with rigid inorganic filler and soft elastomeric inclusions is attained when the filler and elastomer are dispersed separately in the PP matrix. Models for spherical and lamellar particles dispersed in the matrix are shown in Fig. 1.

For spherical elastomeric inclusions in an elastic matrix with perfect bonding between constituents, one may use the Kerner equation calculate the initial elastic modulus of the elastomer-filled matrix, E_{mc} [1]

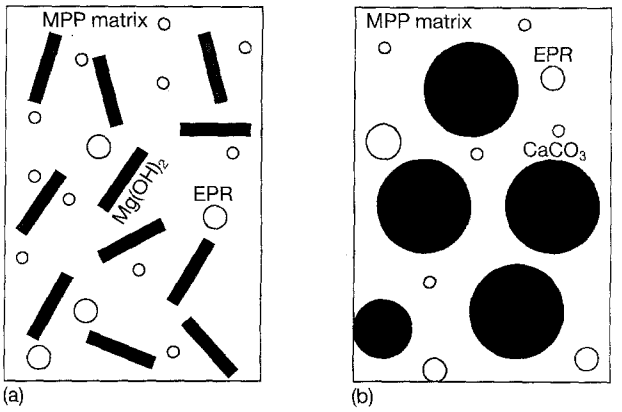

Figure 1 Two-dimensional schematic drawing of the perfect separation case for (a) lamellar and (b) spherical inorganic fillers. $Mg(OH)_2$ is assumed to have square lamellae and $CaCO_3$ with irregular particle shape is assumed to have spherical particles, both lamellae and spheres are monodisperse in size.

$$E_{mc}/E_m = [(1 + ABv_e)/(1 - Bv_e)] \quad (1a)$$

$$A = (8 - 10\,\nu_m)/(7 - 5\,\nu_m) \quad (1b)$$

$$B = (E_e/E_m - 1)/(E_e/E_m + A) \quad (1c)$$

where E_m and ν_m are the modulus and Poisson ratio of the matrix and v_e and E_e are the volume fraction and modulus of the elastomer. The same equation can also be used to calculate the elastic modulus of the composite of an elastomer-filled matrix and an inorganic filler

$$E_c/E_{mc} = [(1 + A'B'v_f)/(1 - B'v_f)] \quad (2)$$

where A' and B' are calculated by replacing ν_m with ν_{mc} and E_e/E_m with E_f/E_{mc} where E_f is the elastic modulus of the filler.

Prediction of the modulus of the lamellar-filled composite is somewhat more complicated because of the geometry of the filler particles. The elastomer-filled matrix is handled in the same way as before using Equation 1. In this work we limit study to a ternary composite with three-dimensional randomly oriented square plates. Particle symmetry considerations lead to the conclusion that this case is identical to that of a composite of two-dimensional randomly oriented fibres in an elastic matrix. One can thus use the Halpin–Tsai equation for the prediction of the properties of unidirectional composites [2] and the Tsai approximation for random orientation of fibres [3]

$$E_c/E_{mc} = \{3/8[(1 + \eta_L\xi_L v_f)/(1 - \eta_L v_f)] + 5/8[(1 + \eta_T\xi_T v_f)/(1 - \eta_T v_f)]\} \quad (3a)$$

where

$$\eta_L = (E_f/E_m - 1)/(E_f/E_m + \xi_L) \quad (3b)$$

$$\xi_L = 2(L/t) \quad (3c)$$

$$\eta_T = (E_f/E_m - 1)/(E_f/E_m + \xi_T) \quad (3d)$$

$$\xi_T = 2 \quad (3e)$$

are the constants characterizing the elastic properties of components and the shape and spatial packing of the filler.

3.2. Lower bound for elastic modulus: perfect encapsulation

A lower bound for the elastic modulus of a ternary composite of PP filled with a rigid filler and elastomeric inclusions is attained when the rigid filler is totally encapsulated in shells of the elastomer component as illustrated in Fig. 2. The formation of rigid core–elastomer shell inclusions reduces sharply the reinforcing efficiency of the filler, thereby leading to a low modulus of elasticity for the composite.

Analysis of this ideal case for lamellar particles is most easily carried out using a finite element analysis (FEA) to evaluate the dependence of the reinforcing efficiency on the thickness of the elastomer interlayer. Two linear FEA packages were used: (i) GT STRUDL for mainframe computers to calculate the dependence of a reinforcing efficiency on the elastic modulus of the interlayer, and (ii) ANSYS 4.4A for SUN4 workstation to evaluate the dependence of the reinforcing efficiency on the thickness of the interlayer. The schematic drawing of the mesh used for FEA calculations is depicted in Fig. 3. Different elastomer volume fractions were represented by different interlayer thicknesses. The reinforcing efficiency, ζ, is calculated as the ratio between the average stress, $\langle\sigma_f^{cs}(L)\rangle$, in an inclusion of aspect ratio of 5 and the maximum achievable stress, $\sigma_f(L \gg L_c)$, in the centre of a long inclusion ($L \gg L_c$) without a soft shell (Calculated at a strain of $\varepsilon = 0.1$ in our case [4, 5])

$$\zeta = \langle\sigma_f^{cs}(L)\rangle/\sigma_f(L \gg L_c) \quad (4)$$

An effective elastic modulus for the core–shell inclusions, E_f^{eff}, is then calculated using a simple rule of mixtures applying the calculated values of ζ [6]

$$E_f^{eff} = \zeta E_f v_f^i + E_e v_e^i \quad (5)$$

where v_f^i and v_e^i are the filler and elastomer volume fraction in the core–shell inclusion respectively, assuming a uniform elastomer interlayer. The calculated effective elastic modulus of lamellar core–shell inclusions ($Mg(OH)_2$/MEPR) as a function of the elastomer volume fraction is shown in Table I.

In the case of spherical particles, the results of Matonis and Small [7] and Matonis [8] for the effect of the soft interlayer on the stiffness of spherical inclusions were used directly to calculate the effective modulus of spherical core–shell inclusions ($CaCO_3$/MEPR). This analysis suggests that for elastomer contents of more than 1–2 vol % filler, a negligible

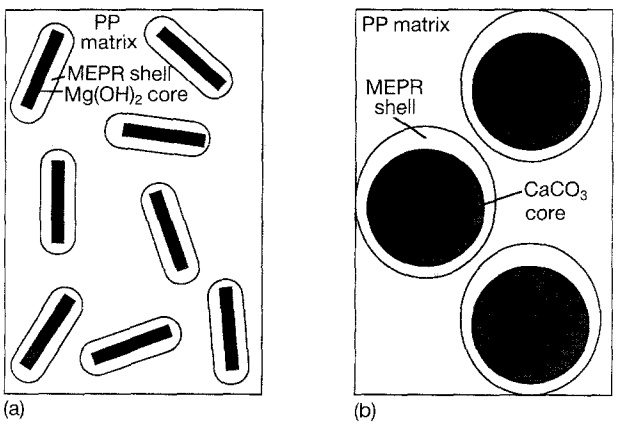

Figure 2 Two-dimensional schematic drawing of the perfect encapsulation case for (a) lamellar and (b) spherical particles. The thickness of the elastomer layer corresponds to about 15 vol % elastomer in a composite with 30 vol % inorganic filler.

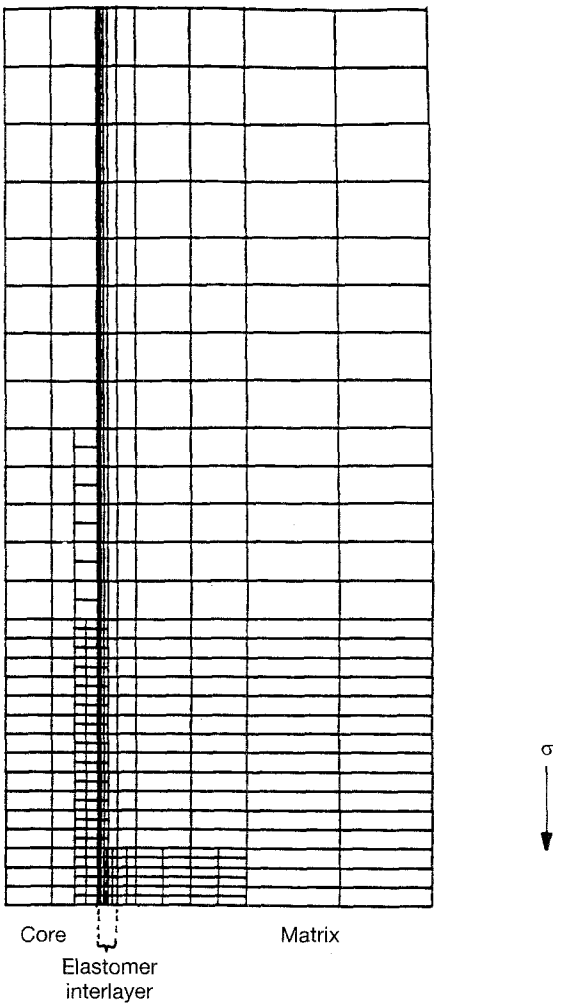

Figure 3 Finite element mesh used to calculate average stresses and, consequently, the reinforcement efficiency factor in a lamellar core–shell inclusion of different elastomer interlayer thicknesses. L/t ratio of the reinforcement was 5, elastic modulus of the rigid core was 64 GPa and that of elastomer was 3 MPa.

Table 1 Reinforcing efficiency ξ of the platelet $Mg(OH)_2$ filler and effective moduli of core-shell $Mg(OH)_2$/MEPR and $CaCO_3$/MEPR inclusions.

Elastomer volume fraction	ξ	Effective modulus E_f^{eff}(GPa)	
		$Mg(OH)_2$	$CaCO_3$
0	0.270	17.3	72
0.01	0.150	9.6	6.5
0.02	0.100	6.0	1.9
0.05	0.055	3.1	0.25
0.08	0.035	1.8	0.05
0.10	0.025	1.2	0.01
0.15	0.020	0.8	0.008
0.20	0.010	0.4	0.004

amount of stress is transferred to the spherical core and the core–shell inclusion behaves principally as an elastomer inclusion with the volume extended by the rigid core. The Kerner equation (Equation 1) is used to calculate the effective modulus. E_{mc} is the effective modulus of the core–shell inclusions, E_m and ν_m are the modulus and Poisson's ratio of the elastomeric shell and E_e and v_e are the modulus and volume fraction of the rigid core. The results are shown in Table I for $CaCO_3$/MEPR inclusions.

The values of effective elastic moduli of core-shell inclusions are used in Equations 2 and 3 to calculate the lower bound of overall elastic modulus, E_c, for the ternary blend with lamellar and spherical core–shell inclusions, respectively. In these cases, the value of E_{mc} is equal to E_m, the modulus of the neat PP, and $v_f' = v_f + v_e$ is the volume fraction of the two-phase, rigid core–soft shell reinforcing inclusions.

4. Results and discussion

4.1. Effect of MAH concentration at constant elastomer and filler volume fractions

4.1.1. Morphology

A set of PP/elastomer/$Mg(OH)_2$ composites containing 30 and 10 vol % $Mg(OH)_2$ and elastomer, respectively, was prepared using [maleated EPR(MEPR)/EPR] blends of different MAH concentrations as the elastomer phase (group I). MEPR adheres strongly to the surface of the filler forming a low-modulus layer around a rigid core. The strength of this bond prevents particles from being easily de-encapsulated by shear forces in the course of compounding. In a second group of samples (group II), [maleated PP (MPP)/PP] blends of different MAH concentrations were used as matrices for ternary composites with $v_f = 0.30$ and $v_e = 0.10$. The presence of MAH in the matrix promotes matrix–filler adhesion and acts in synergy with the shear forces in the melt to prevent the filler particles from being encapsulated by the elastomer.

The contrasting morphologies are shown in the scanning electron micrographs (Fig. 4). Strongly adhered MEPR is less susceptible than unbonded EPR to etching with boiling *n*-heptane. Hence, fewer holes on the etched composite surface of the encapsulated system are visible on the scanning electron micrograph and they are always close to the filler surface. In this case, the thermodynamic adhesion forces acting against shear forces in the melt, promote encapsulation. Owing to the relatively high viscosity of the melt, however, full encapsulation is not reached and some of the filler particles are encapsulated only partially or not encapsulated at all. Because the PP/$Mg(OH)_2$ interface is weak, the propagating crack proceeds along this interface as well as along the PP/MEPR interface. Thus, one can observe filler particles on the fracture surface.

In group II, the adhesion between matrix and $Mg(OH)_2$ becomes stronger than the cohesion of the matrix and, thus, the crack proceeds through the matrix and no $Mg(OH)_2$ particles are visible on the fracture surface. Because the adhesion between MPP and EPR is weak, the crack propagates along an MPP–EPR interface and EPR can be etched off. Spherical holes after the etched elastomer are observed on the fracture surfaces.

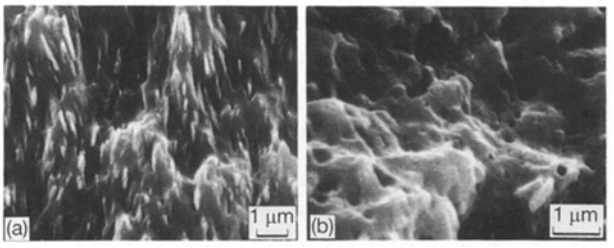

Figure 4 Scanning electron micrographs of the fracture surfaces of ternary composites containing 30 vol % $Mg(OH)_2$ and 10 vol % elastomer in the case of (a) maximum encapsulation and (b) separation achieved at 2 wt % of MAH in the elastomer (a) and matrix (b).

4.1.2. Dynamic moduli

Significant differences between contrasting morphologies are also observed in their dynamic mechanical spectra (Fig. 5), especially in the region of the elastomer glass transition ($T_g^{EPR} = -50\,°C$, $T_g^{PP} = 0\,°C$). The material with core–shell inclusions (group I) exhibits a significantly larger loss maximum at $-50\,°C$, a deeper drop in the storage modulus at $-50\,°C$ and lower values of storage modulus above $-50\,°C$, when compared to the composite with separated rigid and soft inclusions (group II). This result has been attributed to contrasting morphologies in an earlier study on PP/elastomer/$CaCO_3$ composites [9].

4.1.3. Young's modulus

A series of ternary composites of equal composition, (PP/EPR/$Mg(OH)_2$ = 0.60/0.10/0.30), but with increasing concentration of MAH polar groups in either the elastomer (group I) or in the matrix (group II), is analysed. In the case of unmodified polymer components, i.e. PP/EPR/$Mg(OH)_2$, a random array of separated and encapsulated morphologies is achieved resulting from a dynamic equilibrium between thermodynamic forces enhancing encapsulation and shear forces in the melt causing de-encapsulation [10]. Because the acid–base interactions between carboxyls of MAH and hydroxyls of the filler surface are relatively strong [11], the increase in MAH concentration in the matrix phase is expected to enhance the adhesion between MPP and $Mg(OH)_2$ leading to a separation of the filler and elastomer. On the other hand, increasing the amount of MAH in the elastomer phase will enhance the interaction between elastomer and filler, leading to encapsulation of the filler by the elastomer, i.e. the formation of core–shell inclusions.

The transfer of elastomer particles from the bulk matrix to the interlayer on the filler surface (i.e. encapsulation) stiffens the bulk matrix while drastically reducing the reinforcing efficiency of the rigid filler. The net result is a steep reduction in the overall Young's

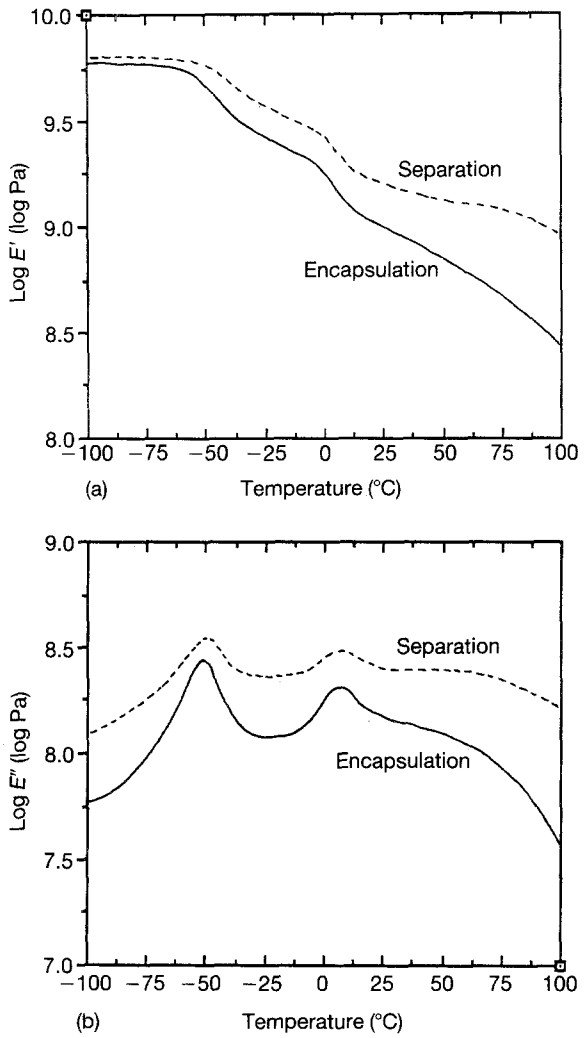

Figure 5 Temperature dependence of (a) the storage and (b) loss moduli for the two contrasting morphologies of ternary composites PP/$Mg(OH)_2$/MEPR (. . . encapsulation). and MPP/$Mg(OH)_2$/EPR (——— separation). Both systems contained 30 vol % $Mg(OH)_2$ and 10 vol % elastomer and maximum achievable content of MAH (2 wt %) in the elastomer and matrix, respectively, at 1 Hz.

modulus of ternary composite, even at constant composition (Fig. 6). A lower limit of Young's modulus (Equations 5 and 3) is approached at the concentration of 2.0 w % MAH in the elastomer phase when nearly all the $Mg(OH)_2$ filler particles are encapsulated by the elastomer.

The increasing concentration of MAH in the PP phase (group II) results in a gradual separation of filler and elastomer and concomitant increase in reinforcing efficiency of the filler and small reduction in the Young's modulus of the matrix. The competition between these two processes results in an increase in the overall Young's modulus of the ternary composite of a constant composition (Fig. 6). An upper limit of Young's modulus (Equation 3) is approached at a concentration of 2 wt % MAH in the matrix when a substantial separation of rigid and soft inclusions occurs.

4.2. Young's modulus – effect of the elastomer volume fraction

As shown previously, one can achieve separation of the filler and elastomer by increasing the adhesion

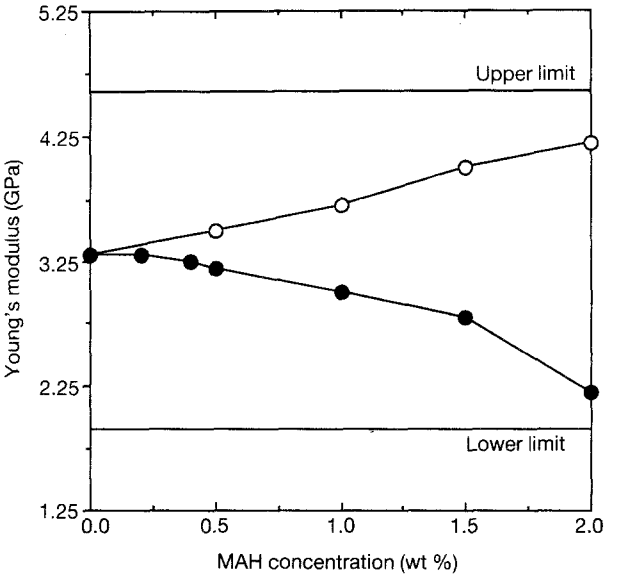

Figure 6 Dependence of Young's modulus on the amount of maleic anhydride in the elastomer ((●) encapsulation) and in the matrix ((○) separation) for a constant composition of 30 vol % $Mg(OH)_2$ and 10 vol % elastomer. Upper and lower bounds are calculated using Equation 3 for the case of perfect separation and perfect encapsulation.

between filler and matrix using maleated PP (MPP) as a matrix. An upper bound of elastic modulus is achieved for the material with perfectly separated secondary components. The effect of elastomer volume fraction, v_e, at a constant filler volume fraction, $v_f = 0.30$, on the values of elastic modulus relative to those for a composite with $v_e = 0$ are shown in Fig. 7. All of the experimental data for MPP/EPR/$Mg(OH)_2$ and MPP/EPR/$CaCO_3$ composites follow the upper bound closely. As predicted from Equations 2 and 3, the moduli for spherical $CaCO_3$ and randomly arrayed square plate $Mg(OH)_2$-filled composites are relatively insensitive to both particle shape and size.

A lower limit of elastic modulus is achieved using maleated elastomer (MEPR) creating core–shell inclusions embedded in a PP matrix. Unlike the upper limit, there is a strong dependence of the lower limit

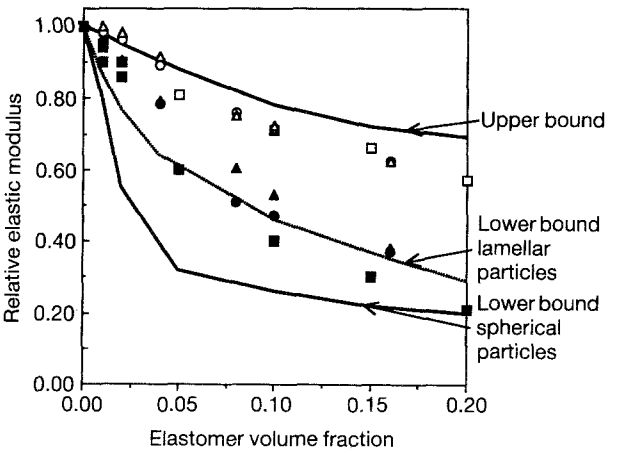

Figure 7 Elastic moduli of ternary composites containing 30 vol % inorganic filler relative to a binary composite ($v_e = 0$). (△, ○, □) Separation (2 wt % of MAH in the matrix), (▲, ●, ■) encapsulation (2 wt % MAH in elastomer). (□, ■) $CaCO_3$; (○, ●) $Mg(OH)_2$, 7 $m^2 g^{-1}$; (△, ▲) $Mg(OH)_2$, 18 $m^2 g^{-1}$.

on the particle shape. The increasing elastomer volume fraction is modelled as an increase in the thickness of a uniform elastomer layer firmly adhered to the filler surface and to the matrix. In the case of lamellar filler, the increase in interlayer thickness reduces the reinforcing efficiency of filler, causing a reduction in the "effective" filler modulus. The values of E_f^{eff} are substituted for E_f in Equation 3 and the resulting composite moduli are plotted in Fig. 7. All the experimental data fall near the lower bound predictions. Fig. 7 shows that the particle size has little effect on the measured moduli. Beyond $v_e = 0.05$, the lower bound prediction is followed closely in the case of $Mg(OH)_2$ fillers. Below $v_e = 0.05$ there is insufficient elastomer to encapsulate all particles, resulting in a higher modulus than the "perfect" encapsulation limit. The $CaCO_3$-filled composites have a lower modulus than the $Mg(OH)_2$-filled composites, but the lower bound was not reached until the elastomer content reached $v_e = 0.2$.

Unlike the case of component separation, where the thermodynamic and shear forces during mixing are working in accord, the thermodynamic forces are acting against the shear forces in the case of filler encapsulation. While almost perfect separation can be achieved under the mixing conditions used, rather complex morphology is achieved when encapsulation is favoured. The relative viscosity of PP and MEPR leads to elastomer particles of the order of 0.5 μm diameter which tend to adhere to the filler surface, creating relatively thick and non-uniform interlayers. Moreover, a portion of the rigid particles remains without any elastomer shell. This is significant, especially at very low elastomer volume fractions. As expected, with the increasing MEPR volume fraction the difference between the lower bound and experimental data diminishes because the amount of particles without elastomer shell decreases, approaching the state of perfect encapsulation.

5. Material design considerations

Figs 8–11 summarize the data on elastic moduli along with experimental measurements of Charpy-notched impact strength (CNIS) at 0 °C. One can thus obtain a clear picture of the compositional range within both the stiffness and toughness of the ternary composites are greater than those of neat polypropylene.

5.1. Constant composition – effect of MAH concentration

5.1.1. Increasing encapsulation

Increasing the concentration of MAH in the elastomer phase causes encapsulation of the filler and, thus, softening of the ternary PP/MEPR/$Mg(OH)_2$ composite (Fig. 8). However, the overall modulus of elasticity remains higher than that for neat PP at the given material composition. CNIS increases significantly with encapsulation being greater than that of neat PP for MAH contents greater than 0.3 wt %.

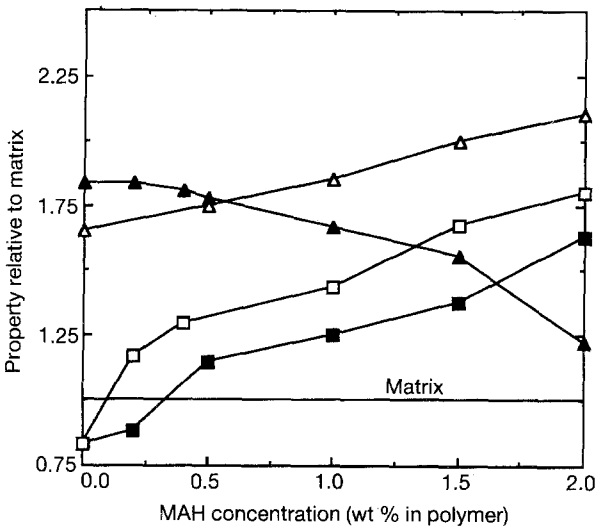

Figure 8 (△, ▲) Elastic moduli (■, □) Charpy notched impact strength at 0 °C relative to those of neat matrix in the case of (△, □) separation and (▲, ■) encapsulation. Filler is $Mg(OH)_2$ with specific surface area of 18 $m^2 g^{-1}$, constant content of filler and elastomer was maintained (30 and 10 vol %, respectively).

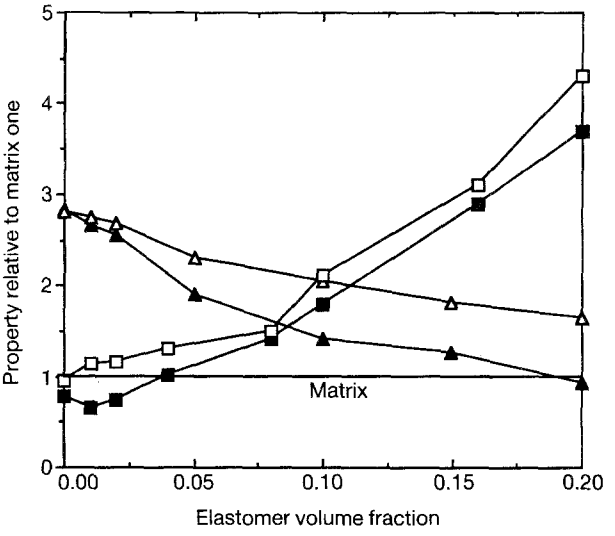

Figure 9 Dependence of the elastic moduli and Charpy notched impact strength (CNIS) of ternary composites relative to those for neat matrix on the elastomer volume fraction in the case of encapsulation and separation. MAH and $Mg(OH)_2$ contents were kept constant equal to 2 wt % and 30 vol %, respectively. Symbols as in Fig. 8. Specific surface area of $Mg(OH)_2$ was 18 $m^2 g^{-1}$.

5.1.2. Increasing separation

Increasing the amount of MAH in the matrix causes separation of the filler and elastomer leading to the stiffening of the ternary material. The CNIS increases with enhanced separation reaching the value for neat matrix at about 0.1 wt % MAH in the matrix (Fig. 8). Observations of the extent of stress whitening and the morphology of the fracture surfaces of the impacted specimens suggest that the mechanism of "toughening" differs from that in the case of encapsulation.

5.2. Effect of the elastomer volume fraction

5.2.1. Encapsulation

The elastomer concentration dependence of the elastic moduli and CNIS for both $CaCO_3$- and $Mg(OH)_2$-filled ternary composites is depicted in Figs 9–11 for

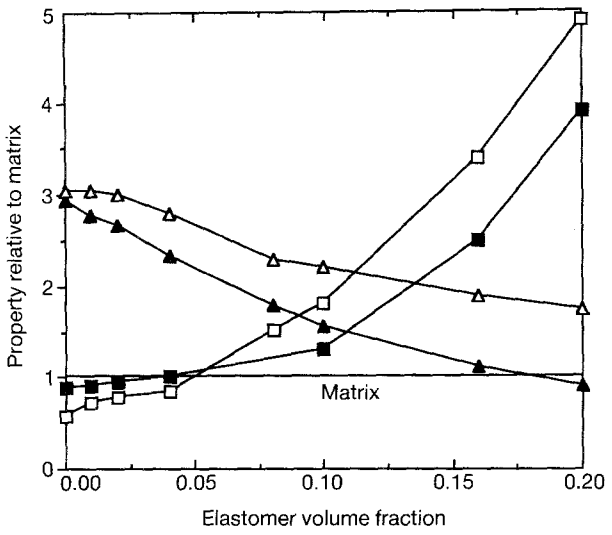

Figure 10 As Fig. 9. Specific surface area of $Mg(OH)_2$ was $7\ m^2\ g^{-1}$.

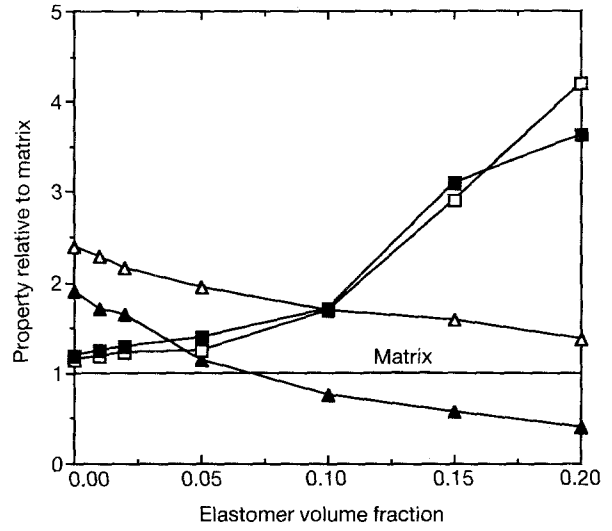

Figure 11 As Fig. 9, with the exception that the filler used was $CaCO_3$ with the specific surface area of $2.6\ m^2\ g^{-1}$.

composites containing 2.0 wt % MAH in the elastomer. The elastic modulus of $Mg(OH)_2$-filled materials is reduced to that of neat PP at about 19 vol % elastomer for $7\ m^2\ g^{-1}$ $Mg(OH)_2$ particles and 15 vol % elastomer for $18\ m^2\ g^{-1}$ $Mg(OH)_2$ particles (Figs 9 and 10), while the CNIS of these composites is greater than that of PP for $v_e > 0.05$. The elastic modulus of the $CaCO_3$-filled ternary composites is reduced to that of PP at 7 vol % elastomer (Fig. 11) while the CNIS is always greater than that of a neat PP. This defines the interval of usable elastomer concentrations in which the materials are both stiffer and tougher than neat PP, namely from $0.05 < v_e < 0.15$ for PP/MEPR/$Mg(OH)_2$ composites and $0 < v_e < 0.07$ for PP/MEPR/$CaCO_3$.

5.2.2. Separation

The modulus of elasticity is, in this case, always greater than that for the neat PP matrix. Despite slight differences in the CNIS between spherical and lamellar fillers, one may conclude that for $v_e > 0.05$ all the materials are both stiffer and tougher than the neat matrix. Differences between particular composites are associated with differences in particle shape and, in the case of $Mg(OH)_2$, particle size. We are presently conducting studies to explore in greater detail the fracture mechanisms in these materials.

6. Conclusions

The relation between elastomer volume fraction and the elastic moduli of PP/EPR/$CaCO_3$ and PP/EPR/$Mg(OH)_2$ ternary composites for the two limiting morphologies, i.e. perfect separation of the filler and elastomer and perfect encapsulation of the filler by the elastomer, were investigated. Simple models for prediction of the upper and lower limits of the concentration dependence of the elastic moduli were proposed, based on existing composite models and finite element analysis. A good agreement was achieved between calculated and experimental data. Both theoretical and experimental results suggest that upper and lower limits of the overall elastic moduli are achieved for perfect separation and perfect encapsulation, respectively. Despite significantly different absolute values of elastic moduli between $Mg(OH)_2$- and $CaCO_3$-filled composites, the concentration dependence of the upper limit for the relative elastic modulus is independent of the particle shape, while the lower limits for spherical and square-plate reinforcement are dependent on particle shape, being significantly higher for the square-plate lamellar particle-filled system.

These findings have some direct implications for industrial material design. One can produce materials with prescribed stiffness and toughness simply by varying either the "degree" of encapsulation or, in the case when a soft interlayer on the filler surface is required, by varying the particle shape or combining particles of different shapes without changing the material composition.

Acknowledgements

The authors thank Chemopetrol, Research Institute of Macromolecular Chemistry for providing the maleated polymers and $Mg(OH)_2$, and Susan M. Connelly for running GT STRUDL FEA calculations.

References

1. L. E. NIELSEN, *J. Compos. Mater.* 1,
2. J. C. HALPIN and J. L. KARDOS, *Polym. Eng. Sci.* **16** (1976) 344.
3. S. W. TSAI and N. J. PAGANO, in "Composite Materials Workshop", edited by S. W. Tsai, J. C. Halpin and N. J. Pagano, (Technomic, Stamford, CT, 1968) p. 233.
4. B. W. ROSEN, Mechanics of Composite Strengthening, in "Fiber Composite Materials", (ASM, 1965) p. 37.
5. L. DILANDRO, A. T. DIBENEDETTO and J. GROEGER, *Polym. Comp.* **9** (1988) 209.
6. L. J. BROUTMAN and B. D. AGARWAL, "Analysis of Performance of Fibrous Composites" (J. Wiley, New York, 1980).
7. V. A. MATONIS and N. C. SMALL, *Polym. Eng. Sci.* **9** (1969) 91.
8. V. A. MATONIS, *Polym. Eng. Sci.* **9** (1969) 100.

9. J. KOLARIK, *Polym. Comm.* **31** (1990) 201.
10. B. PUKANSZKY, F. TUDOS, J. KOLARIK and F. LEDNICKY, *Polym. Compos.* **11** (1990) 98.
11. J. JANCAR and J. KUCERA, *Polym. Eng. Sci.* **30** (1990) 714.
12. C. B. BUCKNALL, *Makromol. Chem., Macromol Symp.* **16** (1988) 209.
13. J. KOLARIK, F. LEDNICKY, J. JANCAR and B. PUKANSZKY, *Polym. Commun.* **31** (1990) 201.
14. J. KOLARIK, F. LEDNICKY, and B. PUKANSZKY, "Proc. 6th Int. Conf. on Compos. Mater." vol 1 (Elsevier, London, 1987) p. 452.
15. J. KOLARIK and J. JANCAR, *Polymer* **32** (1992) 4961.
16. J. JANCAR, A. DIANSELMO and A. T. DIBENEDETTO, *Polymer* **34** (1993) 1684.
17. J. C. HALPIN and J. RAISONI, *Polym. Eng. Sci.* **15** (1975) 183.
18. J. C. HALPIN and J. L. KARDOS, *J. Appl. Phys.* **43** (1972) 2235.
19. L. J. BROUTMAN and B. D. AGARWAL, *Polym. Eng. Sci.* **14** (1974) 581.

Received 7 September 1992
and accepted 27 September 1993